Edge Effect on Eddy Current Detection for Subsurface Defects in Titanium Alloys

*Yibo Wang, Qian Bai, Wei Du, and †Bi Zhang

Key Laboratory for Precision and Non-traditional Machining Technology of Ministry of Education,
Dalian University of Technology, China.

*Presenting author: 344729677@qq.com
†Corresponding author: 15140572053@qq.com

Abstract

Additive/Subtractive Hybrid Manufacturing (ASHM) offers an opportunity for on-line detection due to its layer by layer processes. Eddy current detection (ECD) is a well-established non-destructive method for inspection of surface/subsurface defects in electrically conductive materials. The ECD-enabled ASHM is a promising manufacturing technology to fabricate the parts with good surface condition and material quality. However, edge effect, as an inherent characteristic of ECD, limits the industrial application of ECD. In this study, a specimen with subsurface defects located in the edge area is fabricated. The effects of the edge on ECD signals from subsurface defects are investigated. An effective scanning path is proposed to eliminate the edge effect. A Finite Element (FE) model of ECD is established to analyze the edge effect on ECD. This study provides guidance to determination of the ECD parameters.

Keywords: Eddy current detection; Edge effect; Finite Element; Defects; Reactance

1. Introduction

Additive Manufacturing (AM) offers a great advantage of building parts with geometric complexities. However, defects, e.g. porosities, incomplete fusion holes and cracks, are inevitably introduced if process parameters are improperly chosen. In addition, the current AM methods provide a relatively poor surface finish as well as low dimensional accuracies due to the unstable melt pools. Additive/Subtractive Hybrid Manufacturing, integrating cutting processes into an additive manufacturing process to take advantage of both the simplex AM and subtractive processes, paves a way to enhancing dimensional accuracies as well as removing defects [1]. In laser-based AM processes, optical inspection methods have been investigated by several research groups [2, 3]. The optical methods can detect the abnormal melting pool straightforwardly, however, they provide only limited information on thermal stability and melt pool dimensions during the AM process, and then infer the existence of potential defects indirectly [4].

Eddy Current Detection (ECD), as a non-destructive technique, is widely used to detect surface/subsurface defects of metallic parts, and has a potential application in ASHM. Eddy currents are excited in a test-piece by a magnetic field at a certain excitation frequency [5]. If a defect exists, it perturbs the distribution of the induced eddy currents in the test-piece, and thus manifests localized magnetic anomalies. Therefore, a defect is detected by monitoring the impedance variation of the excitation coil. ECD can avoid the usage of a couplant. In addition, ECD permits high-speed inspection and can be used at elevated temperatures. With portable devices and instantaneous results of ECD, it can facilitate automated in-process inspection. With the limitation of the skin effect and edge effect, ECD is generally applied to detecting defects located away from the edges of a specimen. Besides, the specimen should

have a good surface finish for enhanced detection accuracies [6-10].

Edge effect is an inherent characteristic of ECD. When a detection probe is placed near the edge of a specimen, eddy current flow is perturbed by the edge, which generates mixed signals with that of the defects [10]. The edge effect of ECD has been studied by some investigators. Theodoulidis et al. proposed an analytical model to calculate the electromagnetic field of a cylindrical coil in the edge of a metal block [11]. Bowler et al. developed an expansion method using the truncated region eigenfunction to determine the tangential magnetic field and calculate the impedance of a coil near the edge of a metal plate [12]. Rao et al. combined a multi-frequency eddy current tester with an artificial neural network to eliminate the disturbing variables including the edge effect. They could evaluate the depth of the surface-breaking notches in austenitic stainless steel welds with a maximum deviation of 0.08 mm [13]. He et al. used pulsed the technique of eddy current imaging and frequency spectrum analysis to detect and evaluate the subsurface defects near the edge of a specimen [14]. However, fewer studies are found to cover different detection scanning paths for subsurface defects near the edge.

In order to detect the defects near the edge of a specimen, this paper investigates the effect of edge and defect for ECD signals. The study proposes a method for establishing the effective ECD scanning path to suppress the edge effect and validates the proposed method with ECD experiments and Finite Element (FE) simulations.

2. Experimental setup

2.1 Specimen preparation

In this study, a titanium alloy Ti-6Al-4V specimen with three artificial subsurface defects was fabricated for the ECD experiments, as shown in Fig. 1(a). In order to suppress noise signal of the rough surface, both top and side surfaces were machined. The dimension of the specimen was 40 mm in length, 12 mm in width and 12 mm in height. The subsurface defects are named as Hole #1, Hole #2 and Hole #3, which were prepared by drilling. The diameters of three holes were 2 mm, 1.5 mm and 1 mm, respectively. The depths of all the holes were 2.5 mm from the side surface, and 0.5 mm from the top surface. A coordinate system is built for the convenience to record and analyze data as shown in Fig. 1(b). On the top surface, the x axis coincides with the horizontal centerline of the specimen, and the y axis coincides with the centerline of Hole #3.

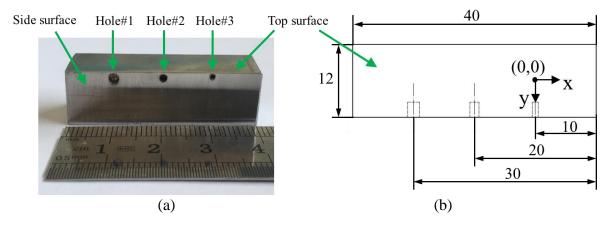(a)   (b)

Fig. 1 (a) Specimen with artificial subsurface defects; (b) Schematic of the specimen in top view. (Unit: mm)

2.2 Experimental setup for eddy current detection

The experimental setup in Fig. 2(a) consists of an eddy current detection setup, a three-axis CNC system, and a three-point levelling platform. In Fig. 2(b), an absolute probe consisting of a copper coil, an interior ferrite core, and an annular ferrite core was used in the experiment. This configuration is able to concentrate magnetic lines around the probe for higher sensitivity and larger depth of detection [15]. The probe has a characteristic inductance L_0=119.96 µH and resistance R_0=5.6 Ω, both in air. Detailed parameters of the probe are listed in Table 1. In ECD, the probe was mounted on a three-axis motion table and moved along the x and y directions. This probe was connected to the eddy current detector to capture electromagnetic inspection data. Signals obtained from a defect-free section of the specimen were set to zero by automatically adjusting the output offset. Detection signals were transmitted to PC for further processing. Detection parameters used in this paper are presented in Table 2.
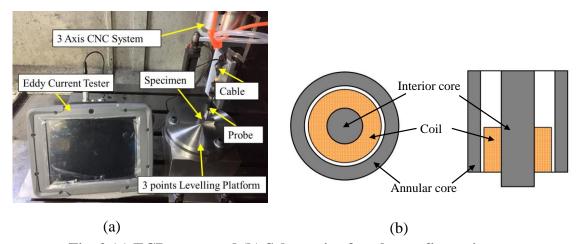

(a)   (b)

Fig. 2 (a) ECD setup and (b) Schematic of probe configuration.

Table 1 Characteristics of the ECD probe

	Inner radius (mm)	Outer radius (mm)	Height (mm)	Turns
Coil	0.80	1.26	1.10	110
Interior core	-	0.76	4.32	-
Annular core	1.40	1.84	3.80	-

Table 2 Detection parameters for ECD

	Lift-off distance (mm)	Scanning speed (mm/min)	Excitation frequency (kHz)	Gain (dB)	Drive voltage (V)
Value	0.05	400	100	60	2.0

3. FE modeling for ECD

In order to study the edge effect on ECD signals, an FE model was established in the ANSYS Maxwell software. Eddy current was calculated based on Maxwell equations, which are defined as follows:

$$\nabla \times E = -\frac{\partial B}{\partial t}$$

$$\nabla \times H = J + \frac{\partial D}{\partial t}$$

$$\nabla \bullet D = \rho$$

$$\nabla \bullet B = 0$$

where E represents the electric field intensity; B the magnetic induction; J the electric current density; D the electric displacement; and ρ the volume charge density.

As shown in Figs. 3(a) and (b), the dimension of the defect in the FE model were set in accordance with the Hole #3. Materials of the coil and specimen were set as copper and Ti-6Al-4V, respectively, interior and annular cores were set as ferrite. The solution type was eddy current, and the excitation frequency was set as 100 kHz. Moreover, the simulation used the natural boundary condition as the default boundary condition, and the solution region was set as 500%. The probe model was set as inside subdivision, the specimen model was set as inside subdivision and skin depth subdivision [16]. The whole model had a mesh number of approximately 88,000. A sample result of the mesh operations is shown in Fig. 3(a).
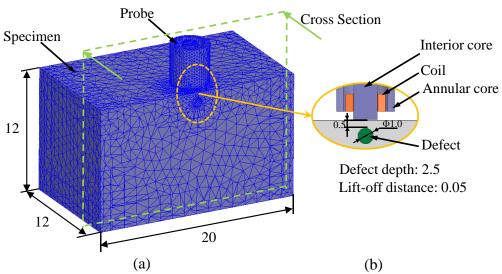

Fig. 3 (a) Meshing of the FE model. (b) Schematics of the cross section of the probe and the defect. (Unit in mm)

4. Results and discussion

4.1 Experiment results

As shown in Fig. 4(a), in top surface, Path 1 passes through the defect-free area between Hole #2 and Hole #3 along the y direction. Path 2 coincides with the centerline of Hole #3 along the y direction. ECD probe was moved along Path 1 and Path 2 in the y direction and the lift-off distance was 0.05 mm.

The reactance signals of Path 1 and Path 2 are shown in Figs. 4(b) and (c). It was difficult to identify the signal of Hole #3 as they were almost similar. Based on the reactance signal of Path 1, the boundary of the edge effect was determined, 3.5 mm from the edge. In Fig. 4(a), Path 3 is along the x direction, and the distance from Path 3 to the edge is 2 mm, which indicates that Path 3 locates in the edge effect area. The reactance signal of Path 3 is shown in

Fig. 4(d). The signal was strong enough to determine the defect locations. For these three defects, peak signals appear corresponding to the defect locations. Furthermore, the signal intensity increases with an increase in the defect size.
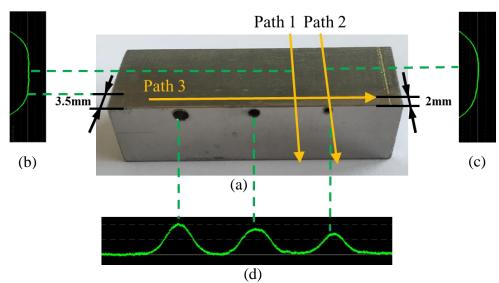

Fig. 4 (a) Specimen with subsurface defects; Screenshot of ECD reactance signal of (b) Path 1; (c) Path 2 and (d) Path 3.

4.2. FE simulation results

Figure 5 shows the normalized signals of reactance and resistance from the FE simulation along Path 1 and Path 2. The normalized factor X_0 and R_0 were the reactance and resistance when the probe was placed at the original point (0, 0). The solid lines and dashed lines represent the signals of Path 1 and Path 2, respectively. The horizontal axis represents the probe position in the *y* direction. Signals of two paths in each figure are very similar, which is in accordance with Figs. 4(b) and (c).
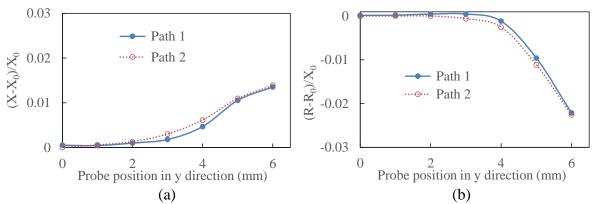

Fig. 5 Comparison of the normalized ECD Signals along Path 1 (solid lines) and Path 2 (dashed lines) simulated by FE (a) Reactance, (b) Resistance.

In order to analyze variations in the eddy current distributions along Path 1 and Path 2 shown in Fig. 6(a), Points A and C were chosen in Path 1, and Points B and D in Path 2. Corresponding to the original point defined in Fig. 1(b), the coordinates of Points A, B, C and D are (-5, 0), (0, 0), (-5, 4) and (0, 4), respectively. Fig. 6(b) shows contours of the eddy current distributions in the FE model.
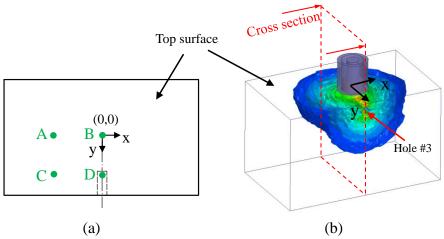
(a)   (b)

Fig. 6 (a) Locations of four points for case study; (b) Contours of eddy current distributions in FE model.

(a)   (b)

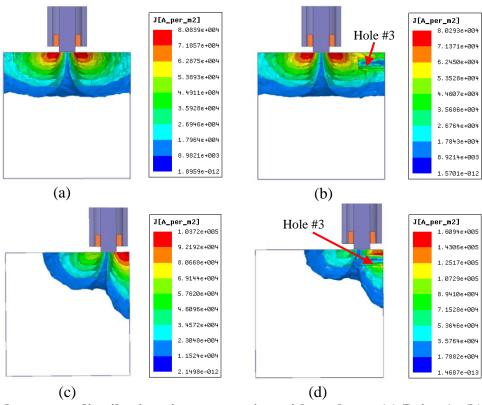

(c)   (d)

Fig. 7 Eddy current distributions in cross section with probe on (a) Point A, (b) Point B, (c) Point C, (d) Point D.

The eddy current distributions for Points A, B, C and D are shown in Figs. 7(a), (b), (c) and (d), respectively. Comparing the eddy current distributions of Points A and C, it is found that when the probe approached the edge above the defect-free area along Path 1, eddy current distribution was only perturbed by the edge effect which influences the ECD signals correspondingly. When the probe approached the edge above Hole #3 along Path 2, as shown in Figs. 7(b) and (d), eddy current distribution was perturbed both by the edge and defect Hole #3. From the results of both the experiment (Figs. 4(b) and (c)) and the FE simulations (Figs. 5(a) and (b)), the signals of Path 2 (the path through defect Hole #3) were similar to those of Path 1 (the defect-free path). Therefore, the influence of the defect is less significant than that

of the edge effect. It is believed that if defects exist in the edge area of the specimen, the signal of defects is difficult to distinguish by ECD when the probe is moved from the central area to the edge area.

Figure 8 shows the normalized signals of reactance and resistance simulated by FE across Hole #3 along Path 3. The normalized factor X_c and R_c were the reactance and resistance when the probe was at Point C. Variations in the signal was observed, which is in accordance with the experimental result. Comparing the eddy current distributions of Point C and D (both located on Path 3), with the existence of Hole #3, the eddy current distribution of Point D was obviously different from that of Point C (as shown in Figs. 7(c) and (d)), which caused the variations in the signal. It is believed that when the probe was moved along Path 3, the edge effect on eddy current distributions can be considered as constant, and the influence of Hole #3 on eddy current distributions could be characterized by the signal variations. Therefore, the parallel motion of the probe along the edge of the specimen enabled ECD to detect defects in the edge area.
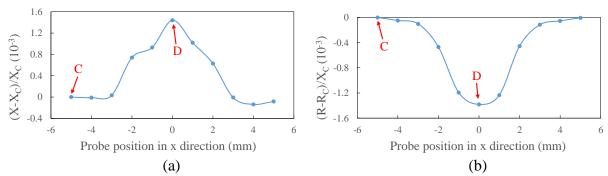

Fig. 8 (a) Normalized reactance and (b) normalized resistance of the ECD Signals from FE simulation across Hole #3 along Path 3.

5. Conclusions

In order to detect the defects near the edge of a specimen, investigations are carried out to reveal the edge effect on ECD signals via experiments and FE simulation. It is found that the signal of defects is difficult to distinguish when the ECD probe is moved from the central area to the edge area. A scanning path parallel with the edge enables ECD to effectively detect the defects near the edge. The peak value of an ECD signal increases with an increase in the defect size even in the edge area.

Further study is recommended to exploiting the capability of the ECD method for ASHM. The study should focus on complex ASHM parts that contain defects of small sizes and different types (e.g., cracks, pores, inclusions, and unmelt powders) in a high temperature environment.

References

[1] Du, W., Bai, Q., & Zhang, B. (2016). A Novel Method for Additive/Subtractive Hybrid Manufacturing of Metallic Parts. *Procedia Manufacturing*, 5, 1018-1030.

[2]   Doubenskaia, M., Pavlov, M., & Chivel, Y. (2010). Optical system for on-line monitoring and temperature control in selective laser melting technology. In *Key Engineering Materials* (Vol. 437, pp. 458-461). Trans Tech Publications.

[3]   Wang, L., Felicelli, S. D., & Craig, J. E. (2007, August). Thermal modeling and experimental validation in the LENS TM process. In *18th Solid Freeform Fabrication Symposium. Austin, TX* (pp. 100-111).

[4]   Kanko, J. A., Sibley, A. P., & Fraser, J. M. (2016). In situ morphology-based defect detection of selective laser melting through inline coherent imaging. *Journal of Materials Processing Technology*, *231*, 488-500.

[5]   García-Martín, J., Gómez-Gil, J., & Vázquez-Sánchez, E. (2011). Non-destructive techniques based on eddy current testing. *Sensors*, *11*(3), 2525-2565.

[6]   Janousek, L., Chen, Z., Yusa, N., & Miya, K. (2005). Excitation with phase shifted fields-enhancing evaluation of deep cracks in eddy-current testing. *NDT & E International*, *38*(6), 508-515.

[7]   Mizukami, K., Mizutani, Y., Todoroki, A., & Suzuki, Y. (2015). Design of eddy current-based dielectric constant meter for defect detection in glass fiber reinforced plastics. *NDT & E International*, *74*, 24-32.

[8]   Vacher, F., Alves, F., & Gilles-Pascaud, C. (2007). Eddy current nondestructive testing with giant magneto-impedance sensor. *NDT & E International*, *40*(6), 439-442.

[9]   Tian, G. Y., & Sophian, A. (2005). Reduction of lift-off effects for pulsed eddy current NDT. *NDT & E International*, *38*(4), 319-324.

[10] Xu, P., Huang, S., & Zhao, W. (2011). A new differential eddy current testing sensor used for detecting crack extension direction. *NDT & E International*, *44*(4), 339-343.

[11] Theodoulidis, T., & Bowler, J. R. (2010). Interaction of an eddy-current coil with a right-angled conductive wedge. *IEEE Transactions on Magnetics*, *46*(4), 1034-1042.

[12] Bowler, J. R., & Theodoulidis, T. P. (2006). Coil impedance variation due to induced current at the edge of a conductive plate. *Journal of Physics D: Applied Physics*, *39*(13), 2862.

[13] Rao, B. P. C., Raj, B., Jayakumar, T., & Kalyanasundaram, P. (2002). An artificial neural network for eddy current testing of austenitic stainless steel welds. *NDT & E International*, *35*(6), 393-398.

[14] Theodoulidis, T. (2004). End effect modelling in eddy current tube testing with bobbin coils. *International Journal of Applied Electromagnetics and Mechanics*, *19*(1-4), 207-212.

[15] Liu, B., Huang, P., Zeng, X., & Li, Z. (2017). Hidden defect recognition based on the improved ensemble empirical decomposition method and pulsed eddy current testing. *NDT & E International*, *86*, 175-185.

[16] Li, Y., Sheng, X., Lian, M., & Wang, Y. (2016). Influence of tilt angle on eddy current displacement measurement. *Nondestructive Testing and Evaluation*, *31*(4), 289-302.